



Dry reforming of methane over a Ni/Al₂O₃ catalyst in a coaxial dielectric barrier discharge reactor

Xin Tu, Helen J Gallon, Martyn V Twigg, Peter A Gorrry, J Christopher Whitehead

► To cite this version:

Xin Tu, Helen J Gallon, Martyn V Twigg, Peter A Gorrry, J Christopher Whitehead. Dry reforming of methane over a Ni/Al₂O₃ catalyst in a coaxial dielectric barrier discharge reactor. Journal of Physics D: Applied Physics, 2011, 44 (27), pp.274007. 10.1088/0022-3727/44/27/274007 . hal-00631679

HAL Id: hal-00631679

<https://hal.science/hal-00631679>

Submitted on 13 Oct 2011

HAL is a multi-disciplinary open access archive for the deposit and dissemination of scientific research documents, whether they are published or not. The documents may come from teaching and research institutions in France or abroad, or from public or private research centers.

L'archive ouverte pluridisciplinaire **HAL**, est destinée au dépôt et à la diffusion de documents scientifiques de niveau recherche, publiés ou non, émanant des établissements d'enseignement et de recherche français ou étrangers, des laboratoires publics ou privés.

Dry reforming of methane over a Ni/Al₂O₃ catalyst in a coaxial dielectric barrier discharge reactor

Xin Tu¹, Helen J. Gallon¹, Martyn V. Twigg², Peter A. Gorry¹, J. Christopher Whitehead¹

¹ School of Chemistry, The University of Manchester, Oxford Road, Manchester, M13 9PL, UK

² Johnson Matthey Plc, Orchard Laboratory, Orchard Road, Royston, SG8 5HE, UK

Corresponding author:

Prof. J. Christopher whitehead

School of Chemistry

The University of Manchester

Oxford Road,

Manchester, M13 9PL

UK

Tel: +44-1612754692

E-mail: j.c.whitehead@manchester.ac.uk

Abstract

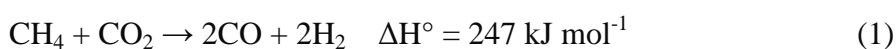
A coaxial double dielectric barrier discharge (DBD) reactor has been developed for plasma-catalytic conversion of CH_4 and CO_2 into syngas and other valuable products. A supported metal catalyst ($\text{Ni}/\text{Al}_2\text{O}_3$) reduced in a methane discharge is fully packed into the discharge region. The influence of the $\text{Ni}/\text{Al}_2\text{O}_3$ catalyst packed into the gas gap on the electrical characteristics of the discharge has been investigated. The introduction of the catalyst pellets leads to a transition in discharge behaviour from a typical filamentary microdischarge to a combination of spatially-limited microdischarges and a predominant surface discharge on the catalyst surface. It is also found that the breakdown voltage of the CH_4/CO_2 discharge significantly decreases when the reduced catalyst is fully packed in the discharge area. Conductive Ni active sites dispersed on the catalyst surface contribute to the expansion of the discharge and enhancement of charge transfer. In addition, plasma-catalytic dry reforming of CH_4 has been carried out with the reduced $\text{Ni}/\text{Al}_2\text{O}_3$ catalyst using a mixing ratio of $\text{CH}_4/\text{CO}_2 = 1$ and a total flow rate of 50 ml min^{-1} . An increase in H_2 selectivity is observed compared to dry CH_4 reforming with no catalyst, while the H_2/CO molar ratio greatly increases from 0.84 to 2.53 when the catalyst is present.

Keywords: Dielectric barrier discharge; Plasma-catalysis; Breakdown; Dry reforming; Hydrogen production

PACS: 52.80.-s, 52.40.Hf, 88.30.-k, 82.33.Xj

1. Introduction

Currently, the demand for effective renewable, alternative energy sources is becoming ever more urgent. The conversion and utilization of abundant low value gases like methane in the form of biogas or landfill gas for the production of fuels and value-added chemicals have exhibited promising potential. The reforming of methane with carbon dioxide, also known as dry reforming, has recently attracted considerable interest due to simultaneous utilization and reduction of two major greenhouse gases, CH₄ and CO₂.



where ΔH° is the standard enthalpy. This process generates synthesis gas (syngas) with a low H₂/CO ratio, which is preferred for the synthesis of valuable oxygenated chemicals and long-chain hydrocarbons. Nevertheless, dry reforming of methane using conventional catalytic methods still faces two major challenges that limit the use of this process on a commercial scale: firstly, high operating temperatures (> 700 °C) are required to obtain reasonable yields of syngas due to the very endothermic reaction (1) and the strength of the C-H bonds in methane, incurring high energy cost; secondly, the formation of severe coke deposition and a subsequent blocking of active metal sites on the catalyst surface, causing rapid deactivation of the catalysts, especially for non-noble metal catalysts [1].

Non-thermal plasma is considered as an attractive alternative for converting greenhouse gases into syngas and other valuable chemicals at lower temperature. Highly reactive species generated in such plasma are favorable for both the initiation and propagation of chemical reactions. Non-thermal plasma has a non-equilibrium characteristic due to a significant difference in temperature between the electrons and heavy particles (ions, atoms, free radicals and excited species). The highly energetic electrons can reach an energy of 1-10 eV, while the

gas kinetic temperature of the plasma can be as low as room temperature, which enables reactions thermodynamically unfavoured to occur at low temperature [2][3]. Several different types of plasma have been investigated for dry reforming of CH_4 over the past decade, most notably, dielectric barrier discharge [4]-[6], atmospheric plasma jet [7], gliding arc [8] and corona discharge [9][10]. Whilst the use of a plasma discharge alone has shown that syngas can be generated at low temperature and atmospheric pressure, the selectivities towards the desired products are typically low. In addition to syngas, significant amounts of higher hydrocarbons ($\text{C}_2\text{-C}_4$), oxygenates, liquid hydrocarbons and polymers can be formed [4][11]. Recently, the combination of plasma and heterogeneous catalysis for fuel production from hydrocarbon reforming has attracted increasing interest [11]-[16]. The interaction of plasma with catalyst could generate a synergistic effect, which might provide a unique way to separate the activation steps from the selective reactions [17]-[22]. Up until now, most of these studies mainly focus on the plasma-catalytic chemical reactions to maximize the process performance [11]-[16], while the interaction mechanisms involved in the combination of plasma with catalyst have received less attention from both physical and chemical perspectives [23]-[25]. The interactions between plasma and catalyst become complex when the catalyst is placed directly in the plasma discharge. Both the chemical and physical properties of the plasma and catalyst can be modified by the presence of each other. Therefore, a better understanding of the plasma-catalyst interactions is required from both a scientific and engineering point of view.

In this paper, we report experimental results on dry reforming of methane in a coaxial double dielectric barrier discharge (DBD) reactor packed with a CH_4 DBD reduced $\text{Ni}/\text{Al}_2\text{O}_3$ catalyst. The effect of packed $\text{Ni}/\text{Al}_2\text{O}_3$ catalyst on the fundamental characteristics of the CH_4

/CO₂ DBD has been investigated through electrical diagnostics. In addition, plasma-catalytic dry reforming reaction has been carried out to examine the activity of the plasma reduced Ni/Al₂O₃ catalyst.

2. Experimental

2.1 Plasma reactor

Figure 1(a) shows a schematic diagram of the experimental setup. The experiment is carried out in a cylindrical DBD reactor consisting of two coaxial fused quartz tubes, both of which are covered by a stainless steel mesh electrode. The inner electrode is connected to a high voltage output and the outer electrode is grounded via an external capacitor C_{ext} (22 nF). The discharge length is 55 mm and discharge gap is fixed at 4.5 mm. CH₄ and CO₂ are used as feed gas with a constant total mass flow rate of 50 ml min⁻¹ and a molar ration of 1:1. The DBD reactor is supplied by an ac high voltage power supply consisting of a function generator (FEEDBACK), audio power amplifier (Europower, EP4000) and high voltage transformer (Amethyst Designs), as shown in Figure 1(b). This power supply provides a maximum peak-to-peak voltage of 22 kV and a variable frequency of 30 - 40 kHz. The applied voltage (U_a) is measured by a high voltage probe, while the total current (I_t) is recorded by a Rogowski-type current monitor (Bergoz CT-E0.5). The voltage (U_c) on the external capacitor is measured to obtain the charge generated in the discharge. All the electrical signals are sampled by a four-channel digital oscilloscope (Agilent DSO6014A, 2GHz). A LABVIEW system is used for the online real-time measurement of discharge power by the area calculation of Q-U Lissajous figure [26]. Images of the discharge are recorded using a high-speed digital camera (Vision Research, Phantom v710).

2.2 Material and products analysis

A commercial catalyst 33 wt. % NiO/Al₂O₃ (Johnson Matthey) is used for plasma-catalytic dry reforming reaction. The unreduced catalyst in the form of NiO/Al₂O₃ is crushed to give non-uniformly sized pellets (18.6 g, 0.85 - 5 mm) and fully packed into the discharge region of the reactor, where it is held in place with quartz wool. Prior to the dry reforming reaction, the reduction of NiO/Al₂O₃ catalyst to metal phase (Ni/Al₂O₃) is performed in a pure CH₄ discharge (50 ml min⁻¹) in the same DBD reactor to activate the catalyst [14]. Then the reduced catalyst (26 wt.% Ni/Al₂O₃) is used for the dry reforming reactions, without removing the catalyst from the reactor after the reduction stage.

A trap cooled by solid CO₂ is placed at the exit of the plasma reactor in order to condense any liquid products. The feed and product gases are analyzed by a two-channel micro gas chromatography (Agilent 3000A) equipped with two thermal conductivity detections (TCD). The first channel contains a Molecular Sieve 5A column for the separation of H₂, CO and CH₄, while the second channel is equipped with a Poraplot Q column for the measurement of CO₂ and C₂-C₄ hydrocarbons. The GC has been calibrated for a wide range of concentrations for each gaseous component by using reference gas mixtures (Agilent Universal Gas Mixture) from Agilent and other calibrated gas mixes.

2.3 Calculation of parameters

Figure 2 shows an equivalent electrical circuit of the DBD reactor. This model consists of two capacitors in a series connection. One of the capacitors C_d represents the total series capacitance of both dielectric quartz tubes and the other is the capacitance for the gap C_g. In the presence of the solid catalyst in the gas gap, C_g represents the contribution of the gas-solid integration in the inter-electrode region. In our study, the equivalent capacitance of the dielectric C_d is 36.2 pF, which is calculated using the coaxial topology of a double quartz

barrier [27]. When the plasma is generated, a resistive channel appears in parallel to C_g . The switch 'K' on the equivalent electrical circuit is fictional.

Figure 3 shows a typical Q-U Lissajous figure for a DBD. Lines BC and DA represent the discharge-off phase when there is only displacement current. The slope of the lines BC and DA corresponds to C_{cell} in the plasma-off period, which is formed by the dielectric capacitance C_d and the capacitance of the gap C_g . The value of C_{cell} can be expressed as

$$\frac{1}{C_{cell}} = \frac{1}{C_d} + \frac{1}{C_g} \quad (1)$$

Thus, the capacitance of the gap C_g in the discharge-off phase can be calculated as follows:

$$C_g = \frac{C_d \times C_{cell}}{C_d - C_{cell}} \quad (2)$$

In the Lissajous figure, lines AB and CD represent the discharge-on phase when the gas breakdown occurs in the gap and plasma is ignited. The slope of these lines is the effective capacitance C_{eff} and should be equal to C_d for a fully bridged gap [28].

The charge Q flowing through the DBD cell can be measured from the voltage drop U_c across an external capacitance C_{ext} (22 nF) according to the relation

$$Q = C_{ext} \times U_c . \quad (3)$$

The voltage on the dielectric material U_d can be obtained from the following equation [29]:

$$U_d = \frac{Q}{C_d} = \frac{C_{ext} \times U_c}{C_d} . \quad (4)$$

Thus the gas voltage U_g across the gap can be given as:

$$U_g = U_a - U_d \quad (5)$$

The breakdown voltage, U_B is the voltage across the gap at which plasma is ignited. U_B can be calculated from the following equation [30][31]

$$U_B = \frac{1}{1 + \frac{C_g}{C_d}} U_{min} \quad (6)$$

The peak to peak charge (Q_{pk-pk}), charge discharged (Q_d) and charge transferred per half cycle (Q_{trans}) are also taken from a measurement of the Lissajous figure as plotted in Figure 3 [29].

For the dry reforming reaction, the conversion rates of CH₄ and CO₂ are defined as

$$C_{CH_4} (\%) = \frac{\text{moles of CH}_4 \text{ converted}}{\text{moles of CH}_4 \text{ input}} \times 100 \quad (7)$$

$$C_{CO_2} (\%) = \frac{\text{moles of CO}_2 \text{ converted}}{\text{moles of CO}_2 \text{ input}} \times 100 \quad (8)$$

The selectivity of the products can be calculated as

$$S_{H_2} (\%) = \frac{\text{moles of H}_2 \text{ produced}}{2 \times \text{moles of CH}_4 \text{ converted}} \times 100 \quad (9)$$

$$S_{CO} (\%) = \frac{\text{moles of CO produced}}{\text{moles of CH}_4 \text{ converted} + \text{moles of CO}_2 \text{ converted}} \times 100 \quad (10)$$

$$S_{C_xH_y} (\%) = \frac{x \times \text{moles of C}_x\text{H}_y \text{ produced}}{\text{moles of CH}_4 \text{ converted} + \text{moles of CO}_2 \text{ converted}} \times 100 \quad (11)$$

$$Y_{H_2} (\%) = \frac{C_{CH_4} \times S_{H_2}}{100} \quad (12)$$

The H₂/CO molar ratio and carbon balance are defined as follows:

$$\frac{H_2}{CO} = \frac{\text{moles of H}_2 \text{ produced}}{\text{moles of CO produced}} \quad (13)$$

$$B_{Carbon} (\%) = \frac{[CH_4]_{out} + [CO_2]_{out} + [CO]_{out} + 2 \times [C_2]_{out} + 3 \times [C_3]_{out}}{[CH_4]_{in} + [CO_2]_{in}} \times 100 \quad (14)$$

The energy efficiency of a plasma reactor for gas conversion is defined as the number of moles of gas converted per unit of plasma power:

$$E = \frac{\text{moles of (CH}_4 \text{ converted} + \text{CO}_2 \text{ converted)}}{\text{Power}} \quad (15)$$

3. Results and discussion

3.1 Effect of catalyst on discharge characteristics

Figure 4 presents electrical signals of the discharge in the mixing of CH₄ and CO₂ with and without Ni/Al₂O₃ catalyst at a fixed discharge power of 50 W. We can see that the total

current of the discharge in the absence of packing catalyst is quasi-sinusoid with numerous superimposed current pulses per half cycle of the applied voltage. These current peaks correspond to filamentary microdischarges in the DBD. In appearance, they are randomly distributed in time and space over the dielectric surface and extend across the discharge gap with an increase of the discharge power. The typical radii of these current filaments have been reported as being in the range of 100 - 200 μm [24][32]. The duration of a single filamentary microdischarge in this case is ~ 10 ns. Therefore, the CH_4/CO_2 DBD without packing material can be characterized as a typical filamentary microdischarge. In addition, it can be seen in Figure 4 that the current pulses are randomly organized in the form of streamer clusters. Most of clusters are composed of a small number of current pulses which overlap in time. The presence of the current clusters indicates a strong interaction character between streamers in the discharge [33]. It is worth noting that the presence of the $\text{Ni}/\text{Al}_2\text{O}_3$ catalyst in the discharge greatly decreases the amplitude of the discharge current but increases the displacement current of the DBD. When the catalyst pellets are fully packed into the discharge gap, the available discharge volume is greatly reduced, effectively limiting the distance over which filamentary microdischarges can form. As a result, only weak filaments can be generated in the void between pellet-pellet and pellet-quartz barrier, as shown in Figure 5(b). We can see the discharges generated between the pellet and quartz wall are much brighter compared to those formed between the pellets. The distance between two pellets or the pellet-quartz wall around their contact points is of primary importance for the generation of filaments. Meanwhile, packing the catalyst pellets into the gas gap introduces a packed-bed discharge effect [18][19], which is characterized by a significant surface discharge on the surface of the packing material. In our case, surface discharges are generated and spread over

the surface of the catalyst pellets due to the packed-bed effect. We can see corona-like discharge around the catalyst surface and the luminance intensity of the surface discharges is much weaker than that of the filamentary discharges generated between the pellet and quartz wall (Figure 5). Our previous studies have shown that increasing discharge power or applied voltage could lead to the expansion of the microdischarge channels transforming into surface discharges in a BaTiO₃ packed bed DBD reactor [34]. Thus, the discharge with fully packed catalyst is a combination of surface discharge on the surface of the catalyst pellets and spatially-limited microdischarges generated in the void space between the pellets and the pellet-quartz wall. The relative contribution of filamentary and surface discharges is likely to depend on many factors including particle size, particle shape and packing location, and hence volume fraction of the packed material in the discharge area. In Figure 5, we can see the spatial distribution of the discharge in the presence of the Ni/Al₂O₃ catalyst is much wider than that of the discharge packed with Al₂O₃. This phenomenon suggests that the conductive Ni active sites on the catalyst also contribute to the spread and expansion of the discharge over the pellet surface. Kim and co-workers have also reported that zeolite-supported metal catalysts assisted the expansion of the discharge over the catalyst surface in a packed bed DBD reactor [24].

In Figure 4, we can also see that the gas voltage of the discharge with catalyst is much lower than that of the discharge without packing. It is worth noting that the breakdown voltage (U_B) decreases significantly with the addition of reduced catalyst from 3.3 to 0.75 kV. This phenomenon can be demonstrated experimentally in that the discharge is much easier to ignite when the reduced catalyst is presented in the plasma reactor. Similar discharge transition behaviour has also been found in our previous studies [25] where the breakdown

voltage for a N₂ DBD packed with zeolite 3A is much lower (1.4 kV) than that for the discharge when no packing material is present (2.3 kV). Guaitella et al have also reported a slight decrease in the breakdown voltage of an air-C₂H₂ discharge when a porous material (<1 mm thick) containing TiO₂ nanoparticles ($\epsilon_r=110$) was placed on the inner surface of the dielectric quartz tube in a coaxial DBD reactor [23]. They suggested that the decrease of the breakdown voltage is mainly due to charge deposited on the dielectric surface and the gas phase modification. Cho et al. have compared the breakdown voltage of discharges using different dielectric barriers in a coaxial DBD reactor [35]. They found that the breakdown voltage between the porous alumina surfaces is only half of the voltage for the discharge between smooth polyimide films even though these two materials have a similar dielectric constant (4.5 for porous alumina and 3.5 for Kapton polyimide film). Large difference in breakdown voltage is ascribed to the transition of the discharge behaviour [35]. In our experiment, the total gas flow rate is kept constant. The size of the catalyst pellets are chosen to be large enough to avoid any pressure drop when packing the catalyst in the DBD reactor. The dielectric constant of the supported metal catalyst (Ni/Al₂O₃) is roughly estimated to be about 50 [36]. Previous observation of a reduction in the breakdown voltage in a nitrogen DBD using different packing materials (Al₂O₃, TiO₂, zeolite 3A) suggests that the influence of gas composition or dielectric constant in the range of $\epsilon_r < 100$ may have played a very minor role on the decrease of the breakdown voltage in our experiment [25]. In our study, we believe that this effect can be attributed to a change in discharge mode in going from typical filamentary discharge to a combination of weak filamentary and predominantly surface discharge when the reduced catalyst is used. An effective decrease of the breakdown voltage can be reached in the surface discharge [37]. Thus the breakdown of gas in the formation of

surface discharge is likely to require a lower breakdown voltage due to the accumulation of charges that occur on the surface of the packing material. The presence of the catalyst pellets in the discharge zone also leads to a significant non-uniformity of the electric field and local overvoltage, especially around the contact points between pellet-pellet and pellet-quartz wall.

The amplitude spectra of the current signals are obtained by means of fast Fourier transform (FFT), as plotted in Figure 6. One prominent peak of 35 kHz is clearly visible in both spectra. This peak originates from the excitation frequency of the high voltage transformer and is independent of any change of the gas flow rate, discharge power and packing material. In addition, another group at around 100 MHz can also be found in the FFT spectra for discharge with and without packing. This frequency is power independent and can be attributed to the lifetime of a single microdischarge (~ 10 ns) in the discharge. The amplitude of this frequency in both spectra is very low. For the discharge with the Ni catalyst, a broad peak at around 12 MHz can be observed, which is directly related to the appearance of a current cluster with duration of 70 - 90 ns in the discharge (Figure 4). However, no prominent peak can be observed for the current clusters in the discharge without packing.

Lissajous figures of the discharge with and without packing material are shown in Figure 7 for a constant discharge power of 50 W. We can see that the shape of the Lissajous figure for the discharge changes from a parallelogram to oval shape when the reduced Ni/Al₂O₃ catalyst is packed in the plasma reactor. This further indicates that physical changes to the discharge mode have taken place. The results in Figure 4 show that despite the constant dissipated power in the plasma discharge, the applied voltage increases from 16.5 kV_{pk-pk}, in the case of no packing to 18.8 kV_{pk-pk} with the Ni/Al₂O₃ catalyst. Given that the discharge power is the same in each case, the current must be smaller in the catalyst-packed plasma discharges,

which can be confirmed from the electrical signals of the discharge (Figure 4).

In the discharge-off phase (lines DA and CB), the total equivalent capacitance of the DBD, C_{cell} , without catalyst is about 7.5 pF, which is independent of the discharge power. This value is also consistent with the capacitance of the DBD cell (7.1 pF) as measured by using a capacitance meter (RS, MEGGER). We can see that this value increases to ~ 18.5 pF when the DBD reactor is packed with the Ni/Al₂O₃ catalyst. In the discharge-off phase, the gap capacitance also increases from 9.5 to 37.5 pF when the catalyst pellets are fully packed into the electrode gap.

Figure 8 shows the effect of packing catalyst on the effective capacitance of the dielectric barrier discharge at different discharge power. The effective capacitance of the DBD (C_{eff}) in the absence of the catalyst increases from 12.7 to 25.2 pF when the discharge power increases from 20 to 60 W. Such evolution is characterized by increasing steeper lines of AB and CD in the Lissajous figure with increase in the discharge power. Similar behaviour of the effective capacitance as a function of the discharge power or applied voltage has also been reported in capillary and surface DBD reactors [38][39]. Francke et al. reported that the effective capacitance C_{eff} should be equal to C_d for a fully bridged gap [28]. In our study, the C_{eff} is much lower than the capacitance of dielectric quartz tubes ($C_d=36.2$ pF) and is power dependent, especially for the plasma without packing. In the absence of the catalyst, we have observed that the microdischarges do not completely cover the dielectric surface in the gap at the discharge power between 20 W and 60 W due to large gap distance and low power density. The discharge extends across the gas gap with the increase of the discharge power. In addition, these phenomena also suggest that the C_{eff} depends on the spatial distribution of the discharge across the gap over a half-period of the applied voltage. When the Ni/Al₂O₃ catalyst pellets

are packed into the gap, we can note that the effective capacitance increases compared to that for the discharge without packing. In our work, packing catalyst into the gap leads to a formation of spatially limited filamentary discharges in the void between the pellets and the pellet-quartz wall. The increase of the C_{eff} in the combination of plasma and catalyst can also demonstrate the presence of the surface discharge in a large area of the gap since the catalyst is fully packed into the gap and the surface discharge can be widely distributed. In addition, we find that the C_{eff} for the discharge with just Al_2O_3 packing (25.8 pF) is much lower than that for the discharge with the $\text{Ni}/\text{Al}_2\text{O}_3$ packing (33.5 pF). This comparison further demonstrates that packing the reduced Ni catalyst into a DBD reactor leads to spatial expansion of the discharge across the gap.

Figure 9 shows the influence of the $\text{Ni}/\text{Al}_2\text{O}_3$ catalyst on the charge generation and transfer in the discharge at different power levels. It can be clearly seen that the peak to peak charge greatly increases with the increase of the discharge power even at a constant applied voltage (16.5 kV) for the discharge without catalyst. Both the charges generated and transferred per half cycle of the applied voltage also increase with plasma power. It is interesting to note that packing the $\text{Ni}/\text{Al}_2\text{O}_3$ catalyst into the discharge gap significantly enhances the peak to peak charge and charge generated per half cycle, which suggests that there is a significant effect of the catalyst on the charge characteristics of the DBD. In addition, we can see that the transferred charge per half cycle for the plasma with catalyst increases by about 10 % in comparison to that for the discharge without packing. It is worth noting that using metal oxide materials (e.g. Al_2O_3) or unreduced $\text{NiO}/\text{Al}_2\text{O}_3$ catalyst in the discharge region decreases the transferred charge per half cycle, which means that non-conductive packing materials in the discharge could inhibit the charge transfer between the electrodes [40]. However, the presence

of the conductive Ni active sites on the catalyst surface acts as a bridge between the electrodes and promotes charge transfer in the discharge due to the increase of charge carrier production and mobility [36]. Moreover, charge is deposited on the gas gap due to the presence of the catalyst. This can also be demonstrated by a larger capacitance value (C_g) of 37.5 pF in the gap, about four times the magnitude of the capacitance with no packing (9.5 pF).

3.2 Plasma-catalytic dry reforming reaction

Plasma-catalytic dry reforming of CH_4 has been carried out with a plasma-reduced Ni/ Al_2O_3 catalyst using a mixing ratio of $\text{CH}_4/\text{CO}_2 = 1$ and a total flow rate of 50 ml min^{-1} . H_2 and CO are the major reaction products, while smaller amounts of acetylene, ethylene, ethane and propane are also formed. Conversions of both CH_4 and CO_2 increase with increasing plasma power as shown in Figure 10. The conversion rate of CH_4 and CO_2 increases up to 18 and 13 %, respectively, at a discharge power of 100 W. Previous modelling and experimental studies have shown that increasing plasma power at a constant excitation frequency effectively enhances the electric field, electron density and gas temperature in the discharge [25][41][42]; all of which may contribute in different ways to the improvement in conversion for both gases. In addition, an increase of power produces more active species, such as O and OH, and can also dissociate CH_4 producing more methyl radicals. With the present plasma-catalyst interaction configuration, the maximum energy efficiency, E , for CH_4 and CO_2 conversion, equaling $0.033 \text{ mmol kJ}^{-1}$ (equation (15)), is achieved at a discharge power of 97 W and a total flow rate of 50 ml min^{-1} . At a higher flow rate, the conversion efficiency can be improved though the conversion rate will be lower. Further improvement of the energy efficiency in DBDs is to be expected from the optimization of the catalyst packing, catalyst

activity and reactor geometry. Our recent work has shown that the energy efficiency for plasma-catalytic dry reforming can be increased by a factor of 8 ($0.23 \text{ mmol kJ}^{-1}$) when Ni catalyst pellet was axially packed along a gap (3 mm in gap width) and activated by an argon-hydrogen plasma [43]. In addition, the energy efficiency of a plasma reactor could be enhanced by a factor of 4 when using rectangular pulses instead of a sinusoidal voltage [44].

At discharge powers between 70 and 100 W, the selectivity towards H_2 increases steadily from 35 to 45 % (Figure 11). This result is greater than the H_2 selectivities obtained in the absence of the catalyst or with any of non-conductive packing materials [40]. The CO selectivities are in the range 18 - 25 % for discharge powers between 70 and 100 W. The selectivities towards CO are much lower than those observed in the absence of a catalyst and for the use of other packing materials, which are in the range 24 - 37 % at a discharge power of 35 W. These results are in contrast to results obtained by Song et al. [15], who found that the H_2 selectivity decreased slightly and the CO selectivity increased when a $\text{Ni/Al}_2\text{O}_3$ catalyst was used during dry reforming of methane at a discharge power of 130 W. In addition, it can be noted that the selectivity of higher hydrocarbon products decreases as plasma power is increased. The maximum C_2 selectivity of 12.4 % can be achieved at a discharge power of 70 W. This suggests that an increase in plasma power leads to a change in the reaction pathways and thus changes the product distribution by converting higher hydrocarbons into more hydrogen. As shown in Figure 12, the highest yield of H_2 (8.2 %) is obtained for the CH_4 plasma-reduced $\text{Ni/Al}_2\text{O}_3$ catalyst, at a discharge power of 97 W.

The carbon balance in the gas stream for the use of catalyst is over 90%. Higher conversions of CH_4 and CO_2 at increased discharge powers are accompanied by higher carbon deposition. As previously described, carbon deposition could be a result of several reactions

including methane decomposition, the Boudouard reaction and possibly electron impact dissociation of other carbonaceous molecules that might produce solid carbon. The formation of H_2 as a percentage of the total gas mixture resembles a mirror image of the carbon balance. Following this observation, it is suggested that methane decomposition to give solid carbon and H_2 is the dominant process that is responsible for carbon deposition during these experiments. The H_2/CO ratio is changed significantly by increased H_2 selectivity and constant CO selectivity. The presence of the reduced Ni/Al_2O_3 catalyst increases the H_2/CO ratio from 0.84 to 2.53 as shown in Figure 13.

In this study, we found that the presence of the Ni/Al_2O_3 catalyst leads to a decrease in conversions of CH_4 and CO_2 in comparison with plasma dry reforming in the absence of a catalyst. Similar observations have been reported in previous studies. Song et al. [15] investigated dry reforming of CH_4 in DBD using a pre-reduced 5 wt. % $Ni/\gamma-Al_2O_3$ in the absence of a diluent gas. The presence of the catalyst had little effect on the CH_4 conversions and on the H_2 and hydrocarbon selectivities. Kraus et al. [16] performed dry reforming of CH_4 in DBD using porous Al_2O_3 foam with a 6 wt.% nickel coating. The yields of H_2 and hydrocarbons were unchanged by the presence of the Ni catalyst. However, CO yields were increased by 20-40 % compared to the results for an uncoated Al_2O_3 foam. These findings lead us to suggest that the physical and chemical interactions between plasma and catalyst may be responsible for the inverse effect of the plasma-catalysis method. Previous studies have also demonstrated that a synergistic effect due to the interaction of plasma and catalyst cannot be generalized to all plasma-catalytic reactions. We believe that the synergistic effect of the combination of plasma with catalysis for hydrocarbon reforming depends on the balance between the change in discharge behavior induced by the catalyst and the

plasma-generated activity of the catalyst. Packing catalyst pellets into the discharge area has been found to shift the discharge behavior from microdischarge in the gas to a combination of surface discharge and weak microdischarges. The relative contribution of filamentary and surface discharges is likely to depend on the volume fraction of the packed material in the discharge area. Such a transition in behaviour of the discharge could reduce the conversions of methane and carbon dioxide, hence the conversion energy efficiency. If the generated surface discharge can increase the activity of the catalyst, the decrease of conversion due to the decrease of discharge current and reduced microdischarges could be compensated for by an improvement in conversion induced by a catalytic effect. However, a strong catalytic effect in the plasma dry reforming reactions could be inhibited or even disappear due to a decrease of catalyst activity or if the catalyst is deactivated by carbon deposition. In this case, the decrease of the conversion by the transition of the discharge behavior cannot be compensated by a catalytic effect, which leads to an overall decrease of the conversion and energy efficiency in the plasma-catalytic process.

4. Conclusion

In this study, plasma-assisted catalysis dry reforming of methane has been investigated using a DBD reactor combined with a plasma reduced Ni/Al₂O₃ catalyst. The introduction of the reduced Ni/Al₂O₃ catalyst into the plasma region significantly changes the physical characteristics of the CH₄/CO₂ discharge compared to that in the absence of the catalyst. The CH₄/CO₂ DBD with no catalyst can be characterized as a typical filamentary discharge, while the discharge with fully packed catalyst is a combination of surface discharges on the catalyst surface and spatially-limited microdischarges generated in the gas-filled space

between the pellets and the pellet-quartz wall. The relative contribution of filamentary and surface discharges is likely to depend on many factors including particle size, shape and their location, and hence the volume fraction of the packed material in the discharge area. It is found that the presence of the reduced Ni/Al₂O₃ catalyst in the discharge greatly decreases the breakdown voltage due to a significant enhancement of local electric field and increased charge deposition on the catalyst surface. We have also shown that conductive Ni active sites dispersed on the catalyst surface contribute to the expansion of discharges and enhancement of charge transfer in the discharge. In addition, we find the presence of the Ni/Al₂O₃ catalyst leads to a decrease in conversions of CH₄ and CO₂ and an increase of H₂ selectivity in comparison with plasma dry reforming in the absence of a catalyst. We have proposed that this effect of plasma-catalyst interaction for reforming reactions can be explained by the balance between the transition in discharge behaviour induced by the catalyst and the durability of the catalyst activity during the plasma catalysis reactions.

Acknowledgement

Support of this work by SUPERGEN XIV – Delivery of Sustainable Hydrogen part of the Energy Programme), the Joule Centre and from the UK EPSRC Engineering Instrument Pool is gratefully acknowledged. The Energy Programme is an RCUK cross-council initiative led by EPSRC and contributed to by ESRC, NERC, BBSRC and STFC.

Reference

- [1] Hu Y H and Ruckenstein E 2004 *Adv. Catal.* **48** 297
- [2] Harling A M, Glover D J, Whitehead J C and Zhang K 2008 *Environ. Sci. Technol.* **42** 4546

- [3] Paulussen S, Verheyde B, Tu X, De Bie C, Marten T, Petrovic D, Bogaerts A and Sels B 2010 *Plasma Sources Sci. Technol.* **19** 034015
- [4] Liu C J, Xue B Z, Eliasson B, He F, Li Y and Xu G H 2001 *Plasma Chem. Plasma Process.* **21** 301
- [5] Sarmiento B, Brey J J, Viera I G, Gonzalez-Elipe A R, Cotrino J and Rico V J 2007 *J. Power Sources* **169** 140
- [6] Wang Q, Yan B H, Jin Y and Cheng Y 2009 *Plasma Chem. Plasma Process.* **29** 217
- [7] Li X, Tao X M and Yin Y X 2009 *IEEE Trans. Plasma Science* **37** 759
- [8] Rueangjitt N, Sreethawong T, Chavadej S and Sekiguchi H 2009 *Chem. Eng. J.* **155** 874
- [9] Li M W, Tian Y L and Xu G H 2007 *Energy & Fuel* **21** 2335
- [10] Ghorbanzadeh A M and Modarresi H 2007 *J. Appl. Phys.* **101** 123303
- [11] Goujard V, Tatibouet J M and Batiot-Dupeyrat C 2009 *Appl. Catal. A: General* **353** 228
- [12] Zhang K, Eliasson B and Kogelschatz U 2002 *Ind. Eng. Chem. Res.* **41** 1462
- [13] Zhang A J, Zhu A M, Guo J, Xu Y and Shi C 2010 *Chem Eng. J.* **156** 601
- [14] Gallon H J, Tu X, Twigg M V and Whitehead J C 2010 *12th Int. Symp. High Pressure Low Temp. Plasma Chem. (Hakone XII)*, Trencianske Teplice, Slovakia
- [15] Song H K, Choi J W, Yue S H, Lee H and Na B K 2004 *Catal. Today* **89** 27
- [16] Kraus M, Egli W, Haffner K, Eliasson B, Kogelschatz U and Wokaun A 2002 *Phys. Chem. Chem. Phys.* **4** 668
- [17] Chen H L, Lee H M, Chen S H, Chao Y and Chang M B 2008 *Appl. Catal. B: Environ.* **85** 1
- [18] Chen H L, Lee H M, Chen S H, and Chang M B 2008 *Ind. Eng. Chem. Res.* **47** 2122
- [19] Chen H L, Lee H M, Chen S H, Chang M B, Yu S J and Li S N 2009 *Environ. Sci. Technol.* **43** 2216
- [20] Istadi I and Amin N A S 2006 *Fuel* **85** 577
- [21] Van Durme J, Dewulf J, Leys C and Van Langenhove H 2008 *Appl. Catal. B: Environ.* **78** 324
- [22] Whitehead J C 2010 *Pure & Appl. Chem.* **82** 1329
- [23] Guaitella O, Thevenet F, Guillard C and Rousseau A 2006 *J. Phys. D: Appl. Phys.* **39** 2964
- [24] Kim H H, Kim J H and Ogata A 2009 *J. Phys. D: Appl. Phys.* **42** 135210
- [25] Tu X, Gallon H J and Whitehead J C 2010 *12th Int. Symp. High Pressure Low Temp. Plasma Chem. (Hakone XII)*, Trencianske Teplice, Slovakia
- [26] Manley T C 1943 *Trans. Electrochem. Soc.* **84** 83
- [27] Valdivia-Barrientos R, Pacheco-Sotelo J, Pacheco-Pacheco M, Benitez-Read J S and

- Lopez-Callejas R, 2006 *Plasma Sources Sci. Technol.* **15** 237
- [28] Francke K P, Rudolph R and Miessner H 2003 *Plasma Chem. Plasma Process.* **23** 47
- [29] Falkenstein Z and Coogan J J 1997 *J. Phys. D: Appl. Phys.* **30** 817
- [30] Kogelschatz U 2003 *Plasma Chem. Plasma Process.* **23** 1
- [31] Wagner H E, Brandenburg R, Kozlov K V, Sonnenfeld A, Michel P and Behnke J F 2003 *Vacuum* **71** 417
- [32] Massines F, Gherardi N, Naude N and Segur P 2009 *Eur. Phys. J. Appl. Phys.* **47** 22805
- [33] Siliprandi R A, Roman H E, Barni R and Riccardi C 2008 *J. Appl. Phys.* **104** 063309
- [34] Tu X, Gallon H J and Whitehead J C 2010 *IEEE Trans. Plasma Sci.* (submitted)
- [35] Cho J H, Koo I G, Choi M Y and Lee W M 2008 *Appl. Phys. Lett.* **92** 101504
- [36] Gomaa M M and Gobara H M 2009 *Mater. Chem. Phys.* **113** 790
- [37] Fridman A 2008 *Plasma Chemistry* (London: Cambridge University Press)
- [38] Mahoney J, Zhu W, Johnson V S, Becker K H and Lopez J L 2010 *Eur. Phys. J. D.* **60** 441
- [39] Kriegseis J, Moller B, Grundmann S and Tropea C 2010 *J. Electrostatics.* (submitted)
- [40] Gallon H J 2010 *PhD Dissertation* The University of Manchester, UK
- [41] Petrovic D, Martens T, van Dijk J, Brok W J M and Bogaerts A, 2009 *J. Phys. D: Appl. Phys.* **42**, 205206
- [42] Li X C, Zhao N, Fang T Z, Liu Z H and Dong L F 2008 *Plasma Sources Sci. Technol.* **17** 015017
- [43] Tu X, Gallon H J and Whitehead J C 2011 *8th Technological Plasma Workshop*, Bristol, UK
- [44] Martens T, Bogaerts A and van Dijk J 2010 *Appl. Phys. Lett.* **96** 131503

Figure captions

Figure 1. (a) Schematic diagram of the experimental setup; (b) High voltage power supply

Figure 2. Equivalent electrical circuit of the DBD reactor

Figure 3. Typical Lissajous figure of a DBD

Figure 4. Electrical signals of the CH₄/CO₂ DBD (a) without packing; (b) with reduced Ni/Al₂O₃ catalyst

Figure 5. Images of the CH₄/CO₂ DBD (exposure time 41 ms) (a) without packing; (b) with reduced Ni/Al₂O₃ catalyst; (c) with Al₂O₃. The arrows indicate some of the regions of discharge when packing is present.

Figure 6. FFT spectra of current signals in the discharge (a) without packing; (b) with reduced Ni/Al₂O₃ catalyst

Figure 7. Lissajous figures of the CH₄/CO₂ DBD with and without reduced Ni/Al₂O₃ catalyst at a constant discharge power of 50 W

Figure 8. Effect of discharge power on the effective capacitance of the CH₄/CO₂ DBD with and without reduced Ni/Al₂O₃ catalyst

Figure 9. Effect of discharge power on charge generation and transfer in the CH₄/CO₂ DBD (a) peak to peak charge; (b) charge generated per half cycle; (c) charge transferred per half cycle

Figure 10. Conversion rate of CH₄ and CO₂ in plasma-catalytic dry reforming reaction

Figure 11. Product selectivities in plasma-catalytic dry reforming reaction

Figure 12. Hydrogen yield in plasma-catalytic dry reforming reaction

Figure 13. Effect of catalyst on H₂/CO molar ratio in plasma-catalytic dry reforming reaction

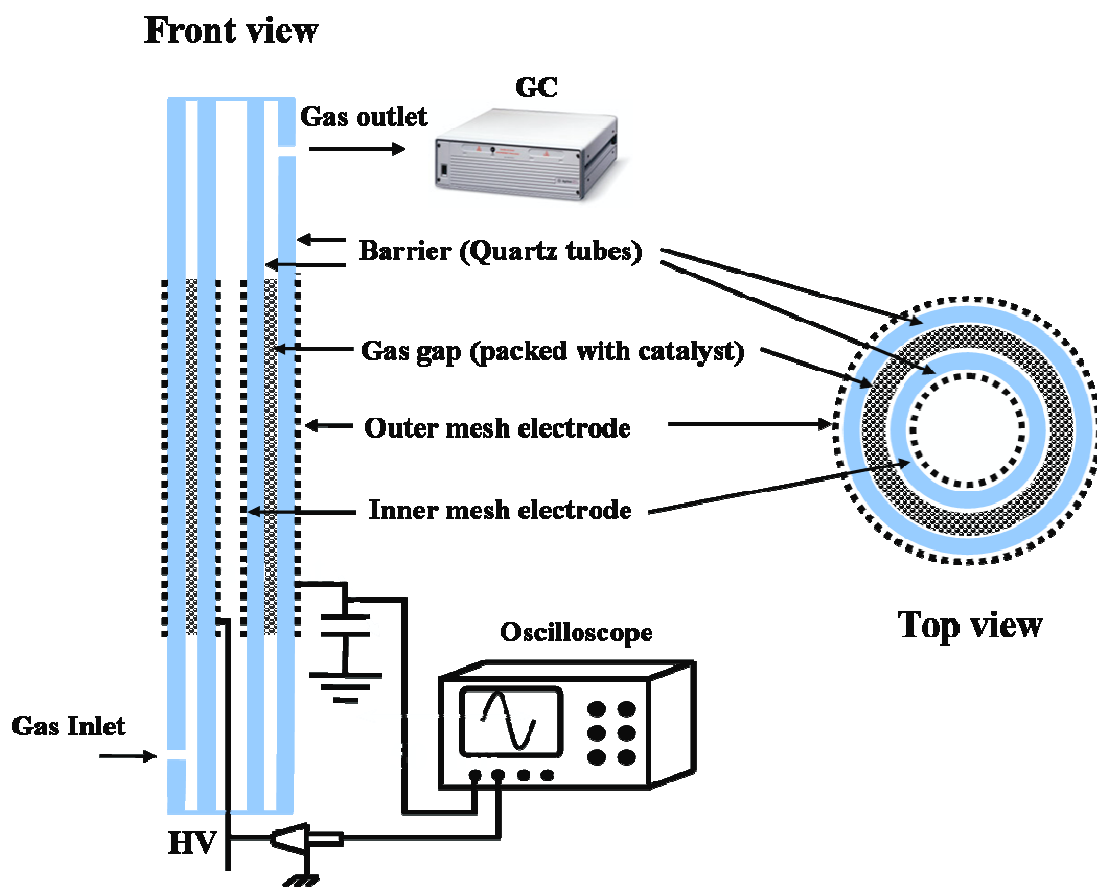


Figure 1(a)

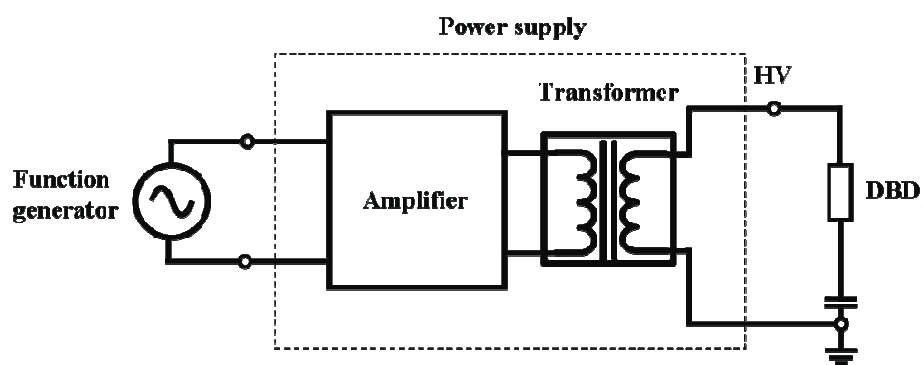


Figure 1(b)

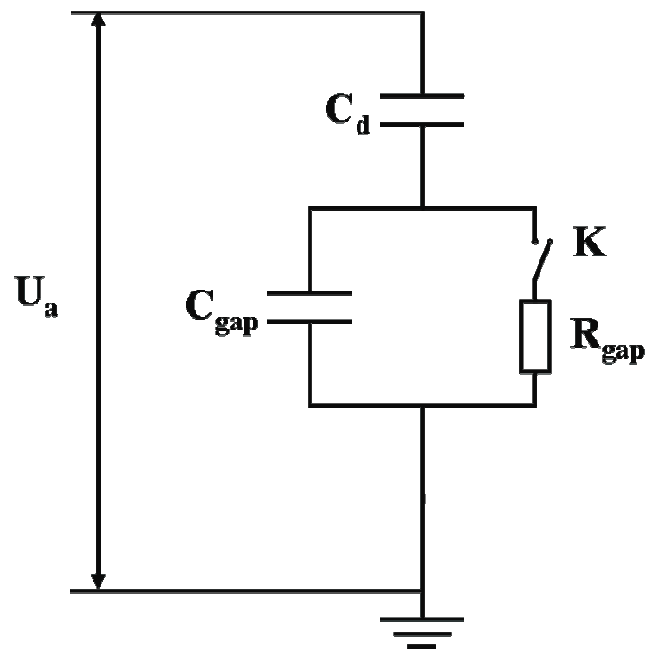


Figure 2

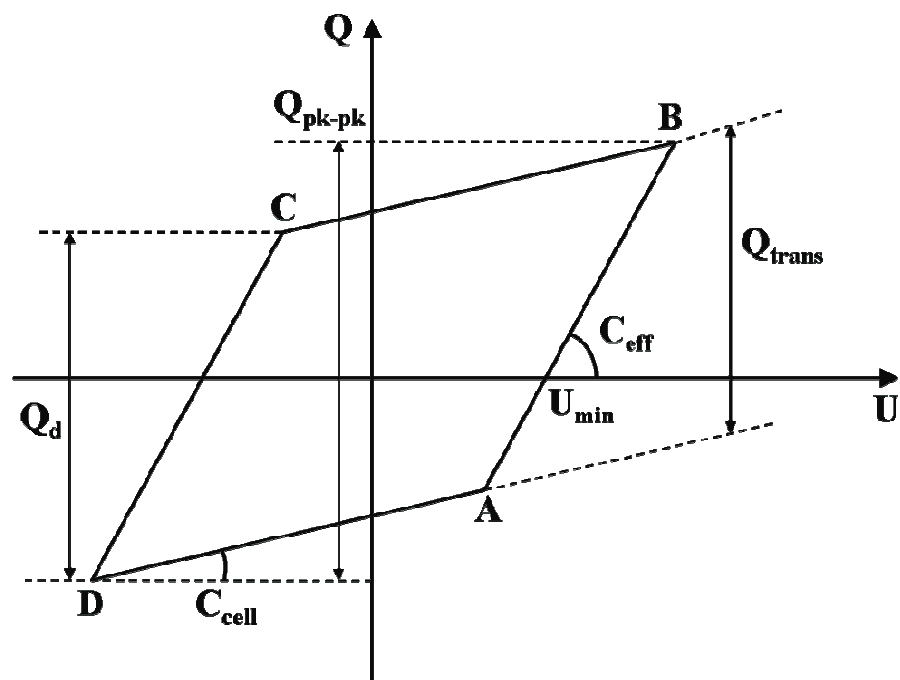


Figure 3

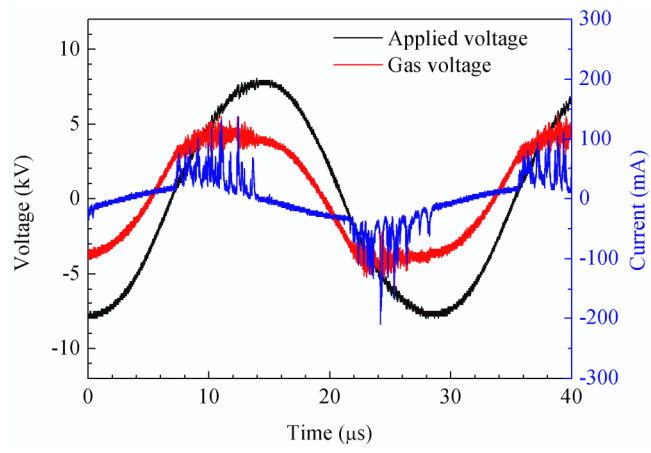


Figure 4(a)

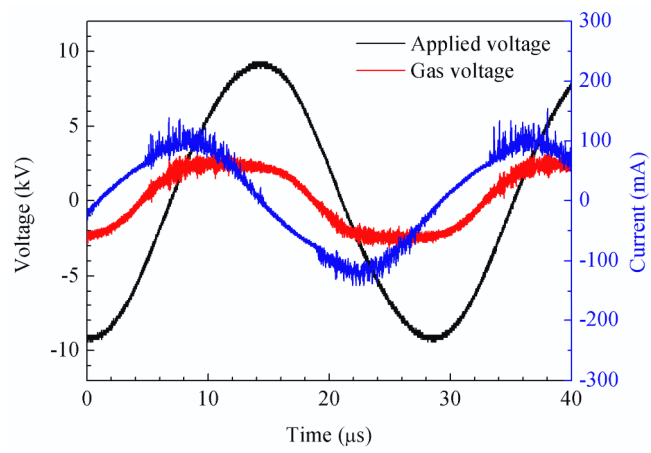


Figure 4(b)

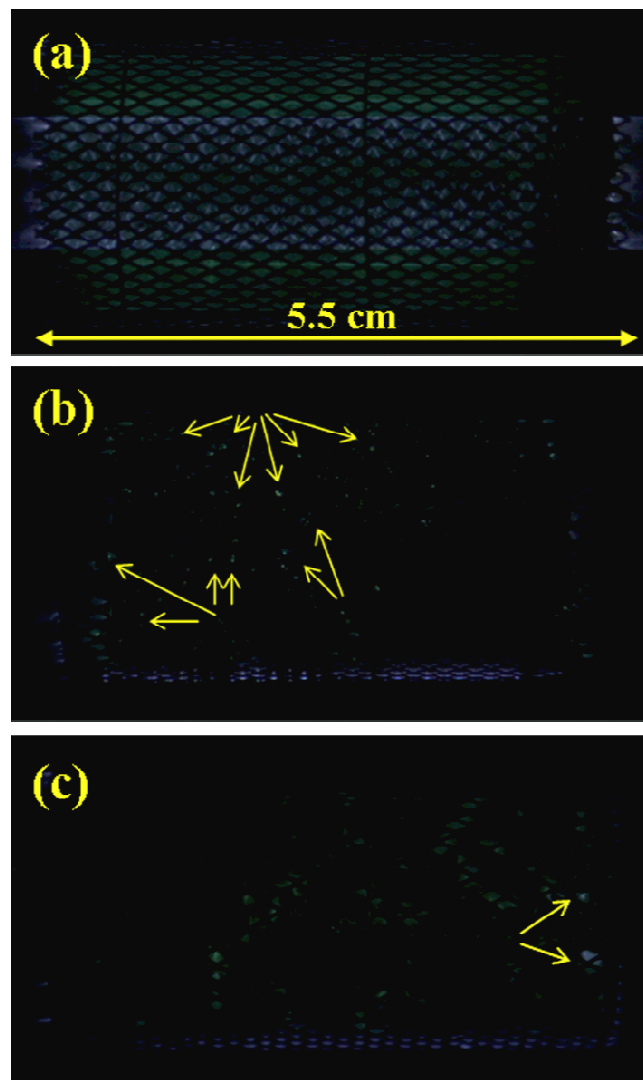


Figure 5

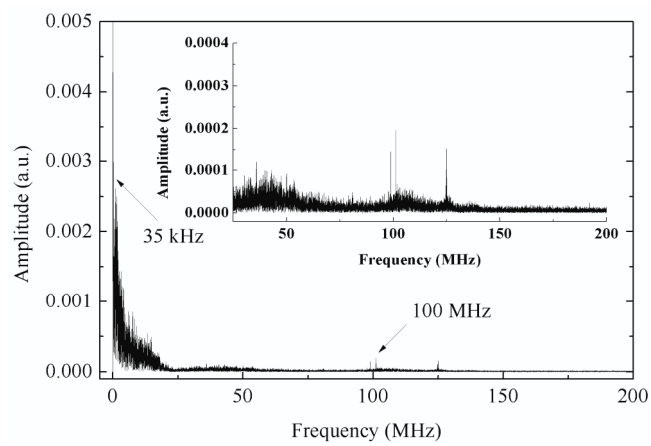


Figure 6(a)

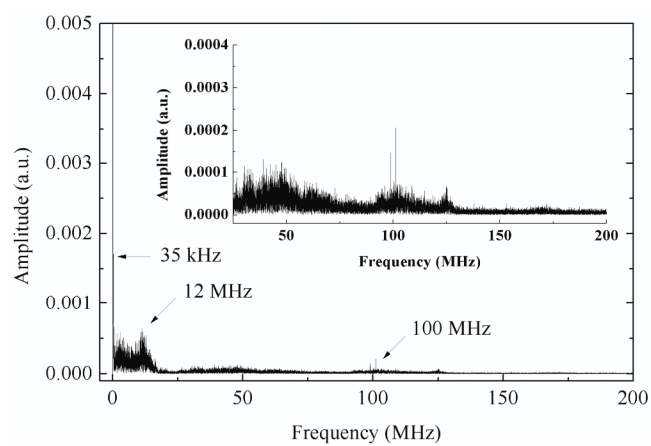


Figure 6(b)

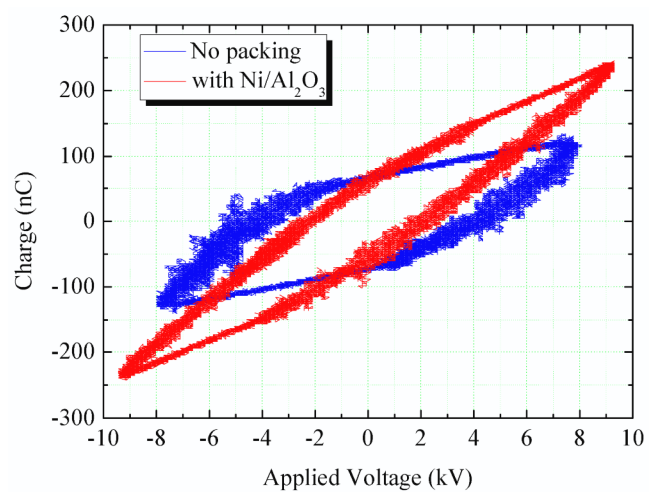


Figure 7

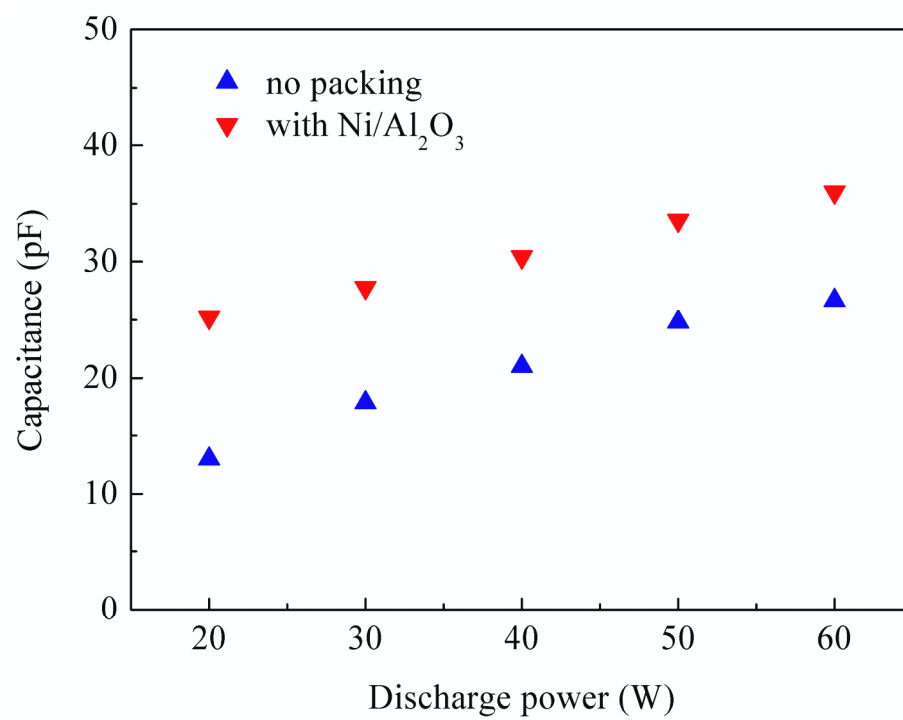


Figure 8

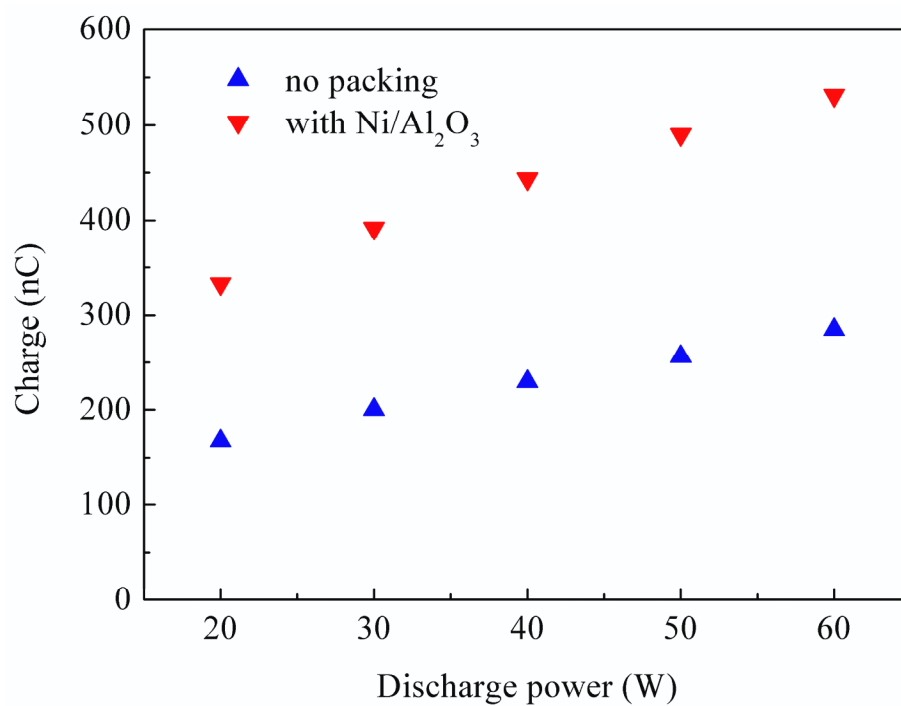


Figure 9(a)

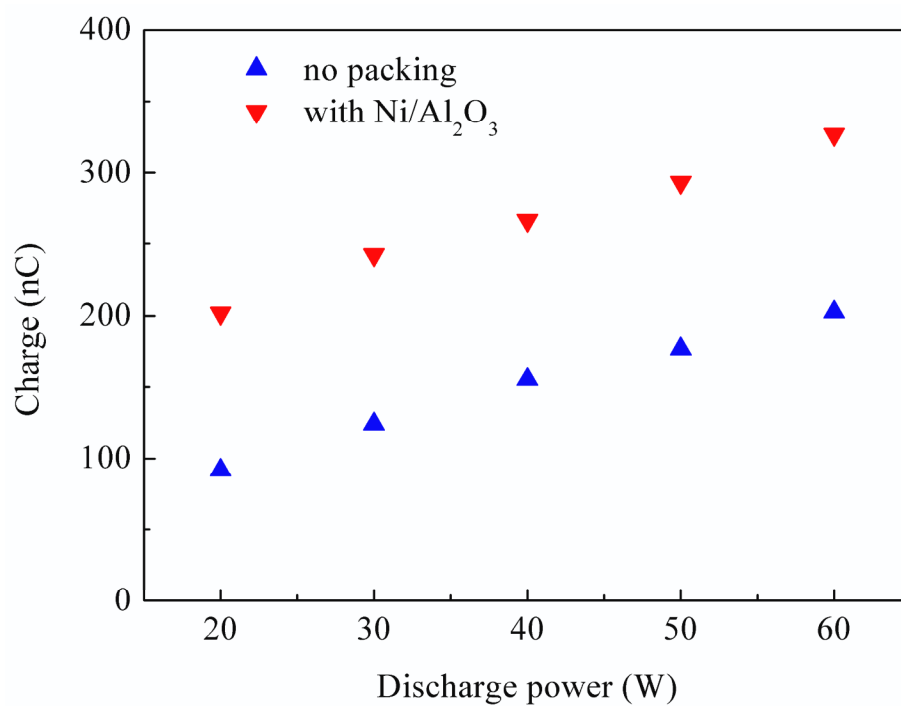


Figure 9(b)

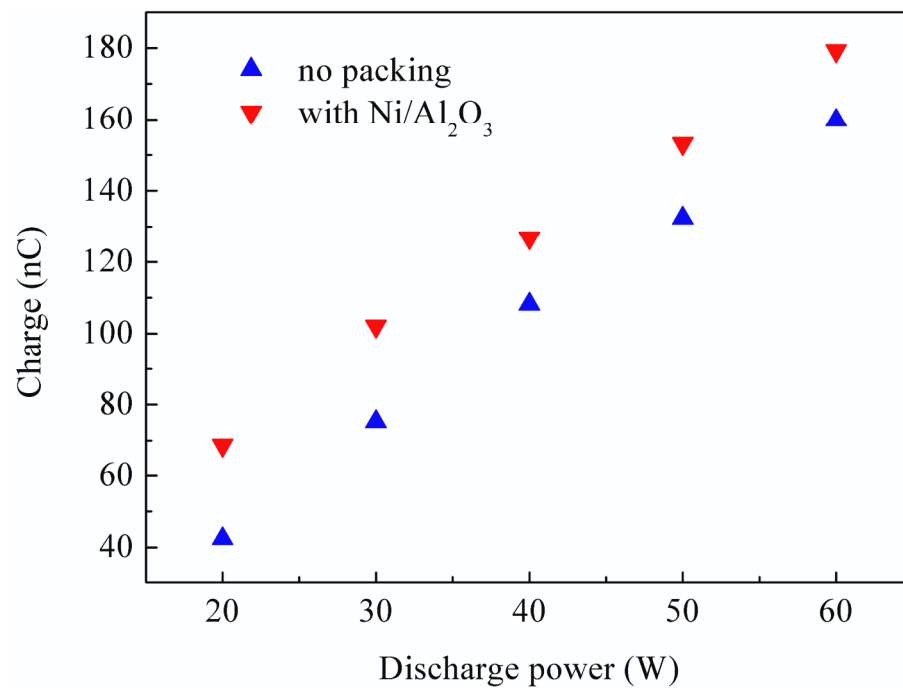


Figure 9(c)

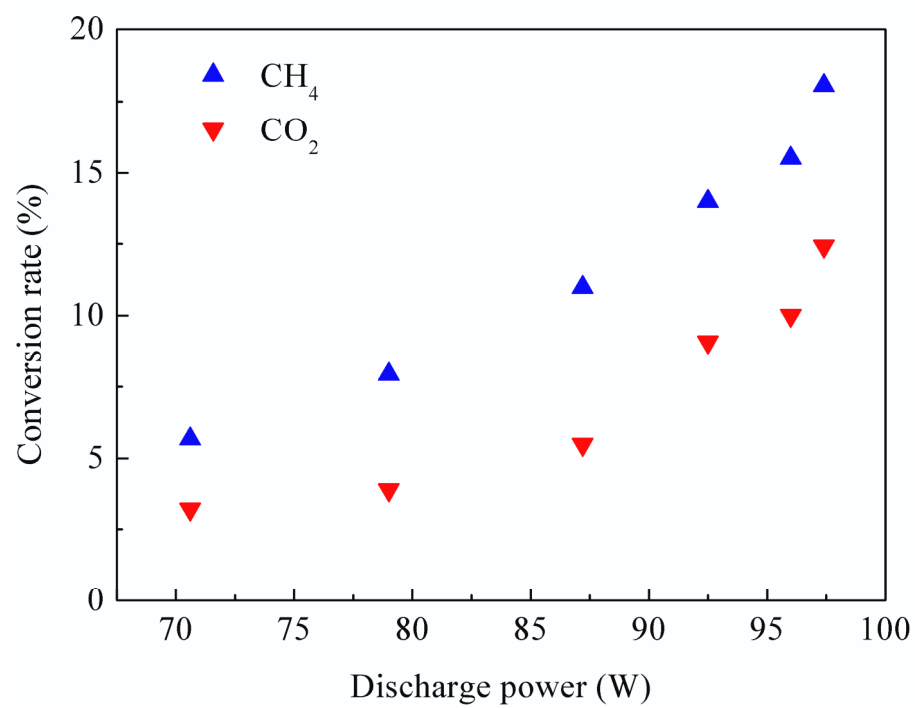


Figure 10

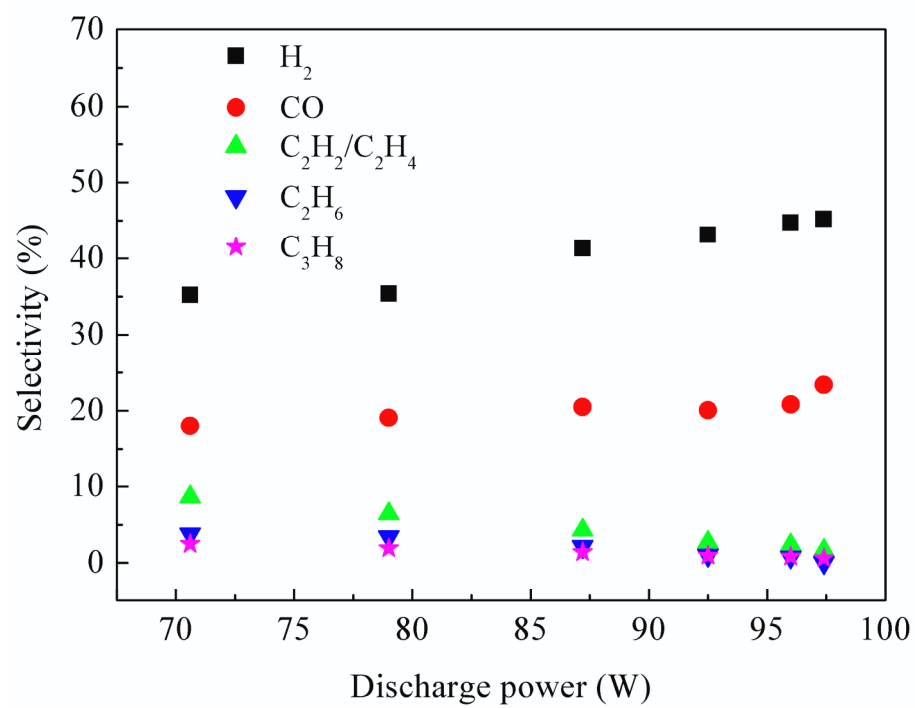


Figure 11

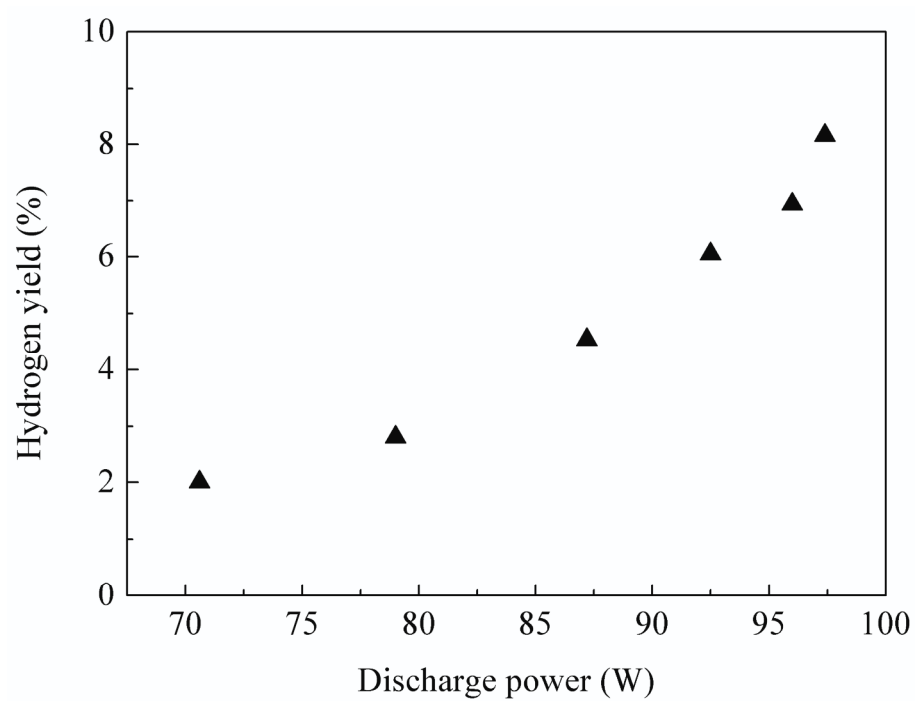


Figure 12

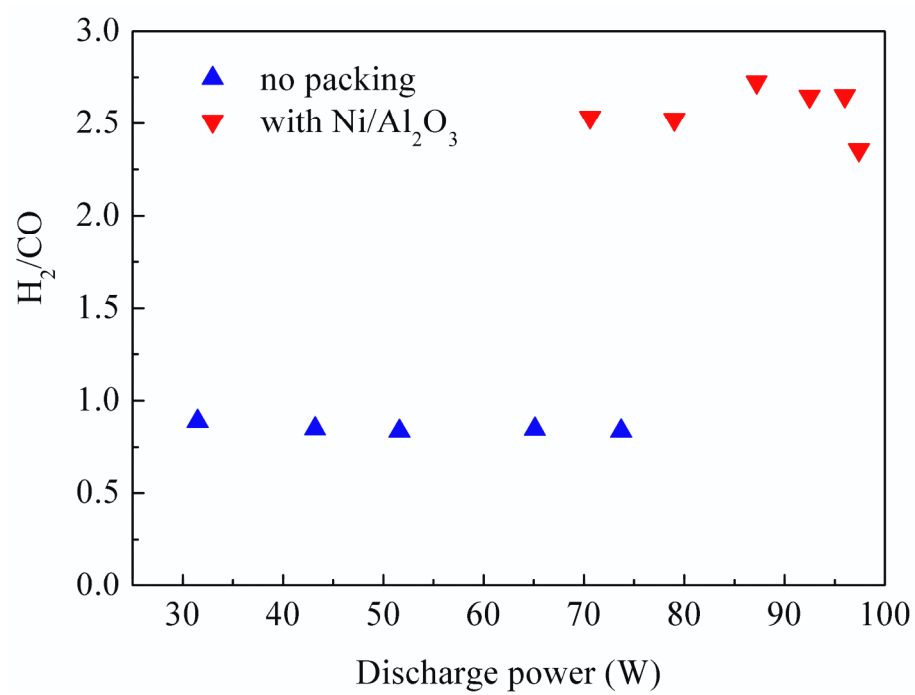


Figure 13